香港科技大學
THE HONG KONG
UNIVERSITY OF SCIENCE
AND TECHNOLOGY

Department of Mechanical and Aeronautical Engineering

Laboratory 2

Numerical Simulation of the Unsteady Flow Around a 2D Cylinder at $\mathbf{R_e = 100\ 000}$

MECH-4830 Introduction to Aerospace CFD

Author: Selim SHERIF
Lecturer : Prof Larry Li
May 12, 2024

Contents

1 Case Setup and Parameters

1.1 Overview

1.1.1 Brief Introduction

The primary objective of the laboratory is to conduct a numerical simulation of unsteady flow around a 2D cylinder, which represents a truck exhaust pipe, utilizing OpenFOAM version 2012. This simulation is performed at a constant Reynolds number of $Re = 100000$. Through systematic experimentation, the aim is to understand the intricacies of non-steady flow simulations and their implications for real-world scenarios. Additionally, there is a focus on exploring various turbulence modeling techniques within computational simulations to gain deeper insights into complex fluid dynamics phenomena, notably vortex shedding.

1.1.2 Engineering Problem and Case Summary

To provide more specific context, the engineering problem being examined involves the analysis of airflow around the vertical exhaust pipe of a standard lorry truck. As the exhaust pipe moves through the still atmosphere, it creates a wake that aims to be analyzed. For the study's parameters, it is assumed that the truck maintains a constant speed of 65 km/h and that the airflow approaching the cylinder remains undisturbed by the truck's frontal shape.
To effectively model this scenario, the problem can be simplified by considering either a vertical cylinder moving through the air or by adopting a frame of reference centered on a stationary cylinder subjected to incoming airflow at 65 km/h as will be done in this study. The following schematic illustrates a summary of the case:

1.1.3 Background

The simplified case presented here reduces to one of the most classic scenarios in the history of fluid mechanics: fluid flow around a cylinder, a quintessential example of flow around a bluff body. Extensively researched, fluid flow around a cylinder exhibits distinct stages, primarily influenced by the Reynolds number. Typically, three stages are characterized:

- **Stage 1:** At low Reynolds numbers, the flow enters the steady laminar creep flow stage, dominated by viscous effects.
- **Stage 2:** Transitioning to the transient stage, instability and unsteadiness become prevalent, giving rise to vortex shedding and the formation of vortex sheets.
- **Stage 3:** Finally, at high Reynolds numbers, inertial effects dominate the flow, rendering it stable once again.

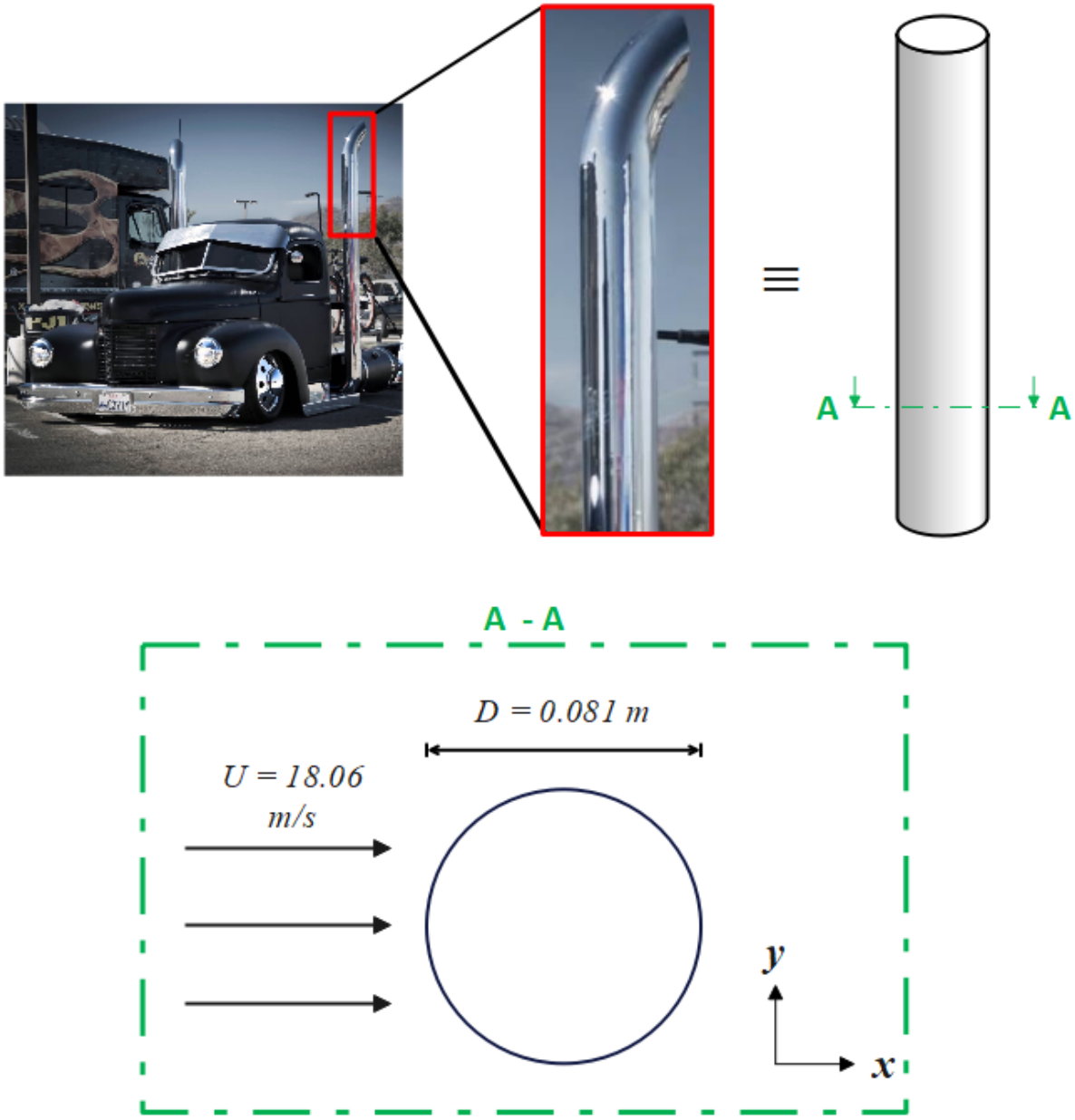

Figure 1: Case Overview

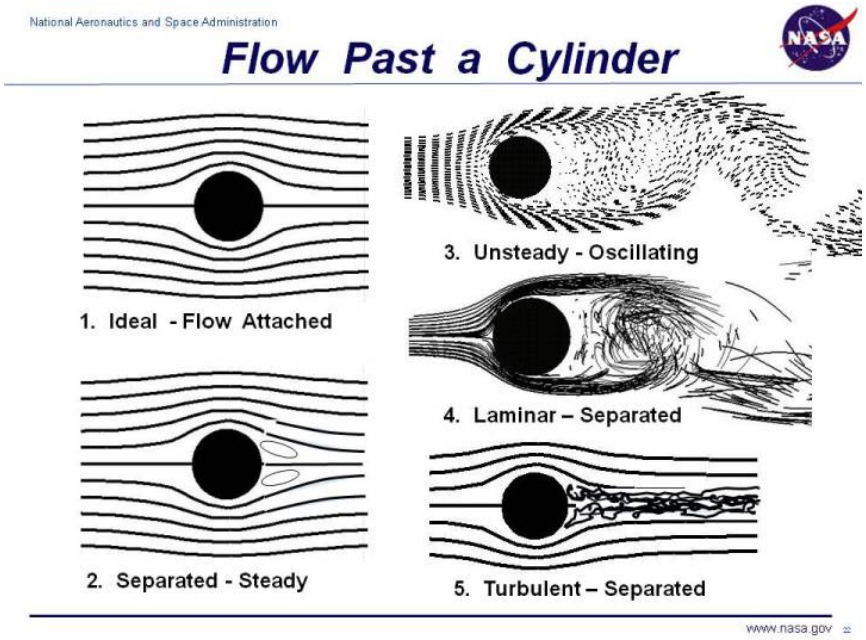

Figure 2: Different flow regimes around a cylinder [1]

In the context of these stages:

- Most practical and physical phenomena are encountered during **Stage 2**, where vortices appear and are observed. In some cases, distinct patterns and symmetries arise during this stage (for example in the case if a cylinder).
- It is important to note that during this stage, a significant parameter of interest is the Strouhal number, which characterizes the pattern and frequency of vortices behind a cylinder. The Strouhal number (**St**) is defined as the ratio of the flow frequency (**f**) to a characteristic length (**D**) divided by the characteristic velocity (**U**):

$$\mathbf{St} = \frac{f \cdot D}{U}$$

- Empirically, the Strouhal number follows a specific relationship within a certain Reynolds number range ($[250; 200000]$):

$$\mathbf{St} = 0.198 * (1 - \frac{19.7}{\mathbf{Re}}) \tag{1}$$

where **Re** denotes the Reynolds number.

1.2 Governing Equations and Underlying Assumptions

The general equations governing fluid flow are as follows:

Mass Conservation: Continuity Equation:

$$\frac{\partial \rho}{\partial t} + \nabla \cdot (\rho u) = 0$$

Momentum Conservation: Navier-Stokes Equation:

$$\frac{\partial (\rho u)}{\partial t} + \nabla \cdot (\rho u \otimes u) = -\nabla p + \nabla \cdot \tau + \rho f$$

Energy Conservation: First Law of Thermodynamics:

$$\frac{\partial (\rho e)}{\partial t} + \nabla \cdot (\rho e u) = -\nabla \cdot (p u) + \nabla \cdot (\tau \cdot u) + \nabla \cdot q + \rho u \cdot f + f \cdot u$$

In this specific case, the flow is defined around a cylinder exposed to a constant airflow. Therefore, the equations can be greatly simplified with the following assumptions:

- **2D Flow**: In this analysis, all terms involving $\frac{\partial}{\partial z}$ are assumed to be negligible, as the flow is independent of the z-axis. Thus, analyzing the flow in the z direction yields equivalent parameters, assuming averaging of all properties. Due to this symmetry, we can directly assume 2D conditions
- **Isothermal Conditions**: Neglecting thermal effects. Therefore, there is no need to use the energy equation.
- **Incompressible Flow**: This means that $\rho = \text{const.}$ and $\nabla \rho = 0$, further simplifying the equations.

With these assumptions the governing equations reduce to:

Continuity Equation (2D Incompressible, Unsteady):

$$\frac{\partial u}{\partial x} + \frac{\partial v}{\partial y} = 0$$

Momentum Equations (2D Incompressible, Unsteady):

- **x-direction momentum:**

$$\rho \left(\frac{\partial u}{\partial t} + u \frac{\partial u}{\partial x} + v \frac{\partial u}{\partial y} \right) = -\frac{\partial p}{\partial x} + \mu \left(\frac{\partial^2 u}{\partial x^2} + \frac{\partial^2 u}{\partial y^2} \right)$$

- **y-direction momentum:**

$$\rho \left(\frac{\partial v}{\partial t} + u \frac{\partial v}{\partial x} + v \frac{\partial v}{\partial y} \right) = -\frac{\partial p}{\partial y} + \mu \left(\frac{\partial^2 v}{\partial x^2} + \frac{\partial^2 v}{\partial y^2} \right)$$

1.3 CFD Solver Choice

With the aim of solving 2D, unsteady, incompressible, and isothermal flows, the optimal approach involves utilizing a pseudo-steady solver to initialize the flow. This process significantly accelerates the simulation, as transient solvers often require extensive time to converge. Utilizing a pseudo-steady state allows bypassing a significant portion of the initial convergence stage, enhancing efficiency.

1.3.1 Pseudo-Steady Solver: SimpleFOAM

For the pseudo-steady solver, **SimpleFOAM** is employed. SimpleFOAM is a robust steady-state solver that is compatible with the previous sections assumptions. We will run the SimpleFOAM Solver for **1500 iterations** before moving to the unsteady solver
Official Description: *SimpleFOAM is a steady-state solver for incompressible, turbulent flow, using the SIMPLE algorithm* [2].
It solves the following equations:

The solver employs the **SIMPLE** algorithm to solve the continuity equation:

$$\nabla \cdot \mathbf{u} = 0$$

and momentum equation:

$$\nabla \cdot (\mathbf{u} \otimes \mathbf{u}) - \nabla \cdot \mathbf{R} = -\nabla p + \mathbf{S}_u$$

Where:

$\mathbf{u}$	=	Velocity
p	=	Kinematic pressure
$\mathbf{R}$	=	Stress tensor
$\mathbf{S}_u$	=	Momentum source

Figure 3: SimpleFOAM equations.

1.3.2 Unsteady Solver: PimpleFOAM

Once the pseudo-steady solution is obtained, it is used to initialize the real unsteady simulation. **PimpleFOAM** serves as an appropriate choice for the unsteady solver. PimpleFOAM can be considered as the older brother of SimpleFOAM. Both PimpleFOAM and SimpleFOAM operate under the same framework, employing the SIMPLE algorithm. However, PimpleFOAM, an extended version of SimpleFOAM, is equipped with the capability to handle transients and a more stable algorithm, known as the PIMPLE algorithm (Which combines the PISO and Simple frameworks).
Official Description: *PimpleFOAM is a transient solver for incompressible, turbulent flow of Newtonian fluids on a moving (or static) mesh* [3] [4].

1.4 Simulation Properties and Parameters

1.4.1 Fluid and Flow Properties

The environmental conditions imposed for this simulation are the ambient conditions. Namely, atmospheric pressure and temperature of $T = 15°\text{C}$
This yields the following properties for air:

Table 1: Fluid, Flow and Turbulence Properties

Parameter	**Value**	**Description**
Fluid And Flow Properties		
Density	$\rho = 1.225$ kg/m^3	Air density
Viscosity	$\mu = 1.79 \times 10^{-5}$ Pa·s	Dynamic viscosity
Kinematic Viscosity	$\nu = 1.46 \times 10^{-5}$ m^2/s	Kinematic viscosity
Temperature	$T = 288.15$ °K	Flow temperature
Reynolds number	$R_e = 1.0 \times 10^5$	Reynolds number Imposed

"It is important to note that two different turbulence models will be used during the simulation: **Spalart-Allmaras** and **K-SST-Omega**. More details will be provided in the relevant subsections. Additionally, both a wall-modeled approach and a wall-resolved approach will be employed, with the parameters clarified in the relevant subsections."

1.4.2 Pressure-Velocity Initial And Boundary Conditions

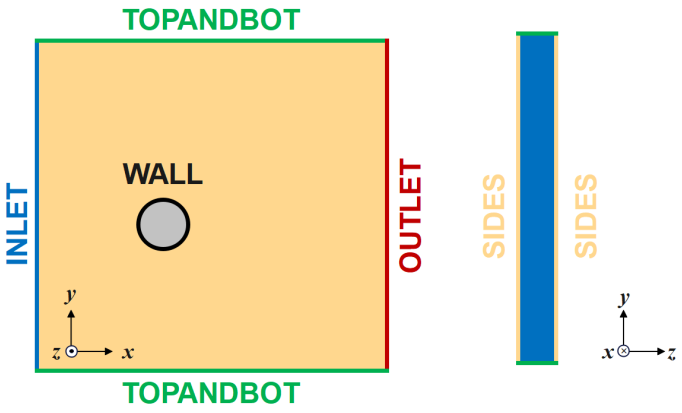

Figure 4: Boundary Names

Table 2: Initial and Boundary Conditions

Parameter	**Value**	**Description**
Initial Conditions		
internalField		
Velocity	Uniform $U_{\mathrm{i}}(0) = (18.06, 0, 0)$ m/s	Uniform unidirectional initial internal velocity field
Pressure	Uniform $P_{\mathrm{i}}(0) = 0$ Pa	Zero initial relative internal pressure
Boundary Conditions		
Inlet		
Boundary Type	Patch	
Velocity BC	InletOutlet $U_{\mathrm{inlet}} = U_{\mathrm{i}}(t)$	Inlet velocity same as local internal velocity
Pressure BC	zeroGradient	Zero pressure gradient normal to inlet patch
Outlet		
Boundary Type	Patch	
Velocity BC	zeroGradient	Zero velocity gradient normal to outlet patch
Pressure BC	InletOutlet $P_{\mathrm{outlet}} = P_{\mathrm{i}}(t)$	Outlet pressure same as local internal pressure
Wall		
Boundary Type	Wall	No fluid can go through cylinder
Pressure BC	zeroGradient	Zero pressure gradient normal to cylinder
Velocity BC	noSlip	Zero velocity at airfoil boundary
Topandbot		
Boundary Type	Patch	
Pressure BC	zeroGradient	Zero pressure gradient normal to top and bottom sides
Velocity BC	zeroGradient	Zero velocity gradient normal to top and bottom sides
Sides		
Boundary Type	Empty	No solving of equations across sides
Pressure BC	empty	
Velocity BC	empty	

2 Grid Convergence Test and Mesh Selection

The general mesh setup has the following shape. It's important to note that, during the GCT, we will be using the following turbulence and flow properties :

Table 3: Turbulence Model : GCT (See 11 for more details)

Parameter	**Value**
Turbulence Model	SpalartAllmaras
Turbulent Viscosity (ν_t)	1.4×10^{-5} m^2/s
$\tilde{\nu}$ (Nutilda)	5.5×10^{-5} m^2/s
Boundary Layer Solution	Wall Resolved

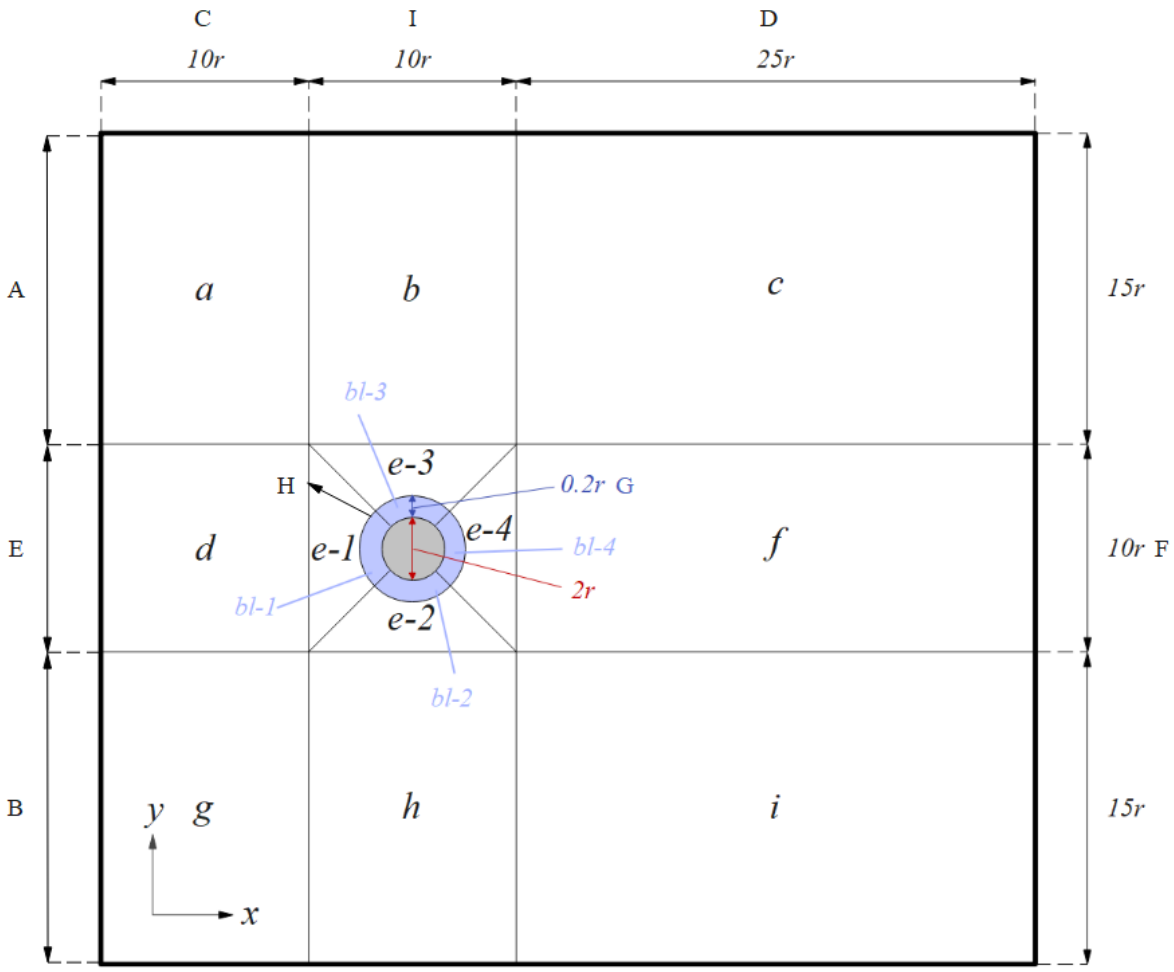

Figure 5: Mesh basic setup

4 progressively finer meshes are used throughout the grid convergence test in order to find a good balance between computational efficiency and numerical accuracy:

Mesh	**A**	**B**	**C**	**D**	**E**	**F**	**G**	**H**	**I**	**# of Cells**
Point Distribution Parameters										
Coarse	16	16	16	75	36	36	16	36	36	13835
Medium	21	21	21	100	51	51	24	51	51	27310
Medium-2	30	30	30	150	60	75	29	65	70	51995
Fine	45	45	25	200	70	120	35	90	100	101151
Progression Parameters										
Coarse	1.15	1.15	0.9	1.01	1.0	1.0	1.335	1.04	1.0	–
Medium	1.12	1.12	0.92	1.005	1.0	1.0	1.182	1.03	1.0	–
Medium 2	1.06	1.06	0.95	1.002	1.0	1.0	1.138	1.03	1.0	–
Fine	1.035	1.035	0.91	1.004	1.0	1.0	1.104	1.022	1.0	–

Table 4: Mesh Parameters

The progression G has been strategically chosen such that the height of the first cell l_0 does not change with the different mesh granularity.
After Conducting the simulations with all the different meshes, the following results are obtained:

Table 5: Grid Convergence Study Results

Mesh	C_d **(% Change)**	S_{t_L} **(% Change)**	$\theta_{\textbf{sep}}$ **(% Change)**	**Comp. Time (core-hours)**
Coarse	0.6213 (–)	0.2446 (–)	101.2 (–)	24.7
Medium	0.6010 (3.38%)	0.2446 (0%)	103.0 (1.75%)	34.0
Medium-2	0.5937 (1.23%)	0.2431 (0.63%)	103.7 (0.68%)	78.1
Fine	0.5919 (0.3%)	0.2422 (0.38%)	104.1 (0.38%)	190.6

We can interpret the following from the results:

- The time-averaged drag follows an expected exponential shape, gradually decaying and converging to a certain value, with the relative errors decreasing in a diminishing manner. This trend can be observed in the following plot:

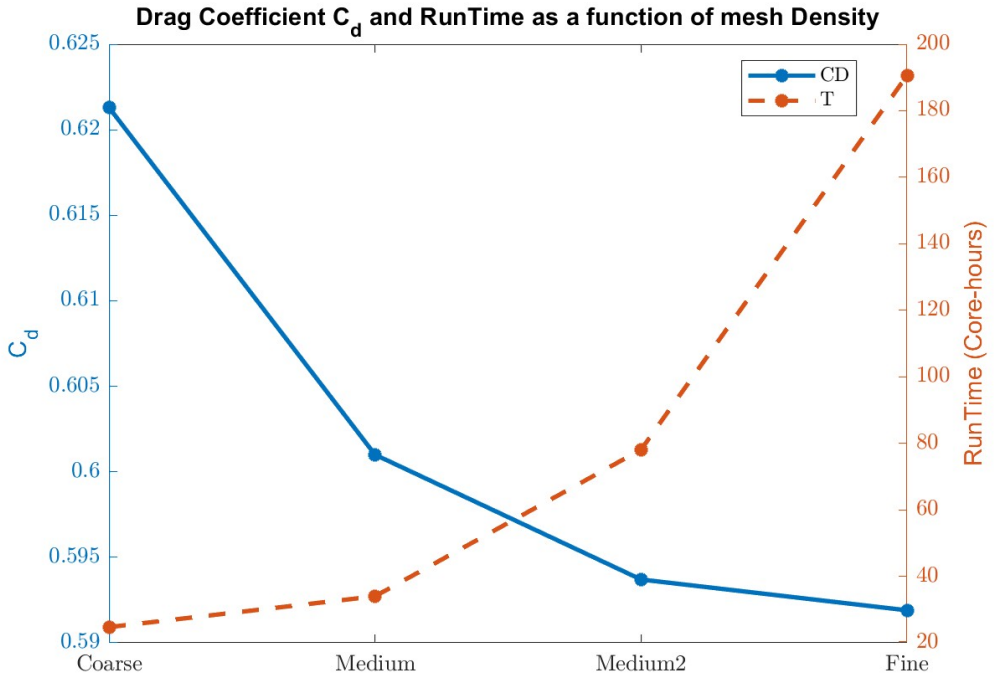

Figure 6: GCT: Drag Coefficient and Runtime

- The general trend for the Strouhal Number is a decreasing behavior with progressively finer meshes. However, this result must not be overstated or overemphasized because the frequencies used in the Strouhal number computation are extracted from an FFT algorithm. The FFT is a discrete model, meaning it is an approximation that yields a margin of error. In this case, the margin of error is significant enough to alter the interpretation of the result.

- The angle of separation is extracted visually using ParaView. The general trend here is that the finer the mesh, the larger the separation angle. This makes sense because the finer mesh captures more detail compared to a coarser one, meaning it can capture more precisely what is happening in the boundary layer.

Overall, there are 2 meshes that seem to be good for the job: the medium**Medium** mesh and the **Medium-2** mesh. Both strike a delicate balance between computational efficiency and numerical accuracy, although the medium 2 mesh slightly emphasizes numerical accuracy over efficiency. The optimal mesh chosen for the simulations is the Medium 2 mesh in the spirit of being cautious rather than taking risks. However, in practice, both the Medium mesh and the Medium 2 mesh would make great choices.

3 Effect of CFL Number

3.1 Understanding the CFL Number

When dealing with transient unsteady flow CFD, a delicate balance must be struck between the time step of each discrete iteration and the length of every computational cell. If the time step is too large, the flow may "skip" certain cells, potentially leading to inaccuracies in the simulation. To consider this, an additional parameter must be monitored, described by the Courant-Friedrichs-Lewy (CFL) number, which ensures the stability and accuracy of transient simulations.

The CFL number is defined as the ratio of the characteristic flow velocity (u) to the characteristic length scale (Δx) divided by the time step (Δt):

$$CFL = \frac{u \cdot \Delta t}{\Delta x}$$

It's important to note that, as is common in CFD, there exists a compromise between numerical accuracy and stability, as well as computational time and resources. Generally, CFD engineers should aim to keep the Courant number under 1. This ensures that all the information of the flow is captured in each computational cell, thereby preserving the integrity of the simulation.

The goal of this section is to experiment with the CFL number to observe its effects on transient unsteady flow simulations, exploring how variations in the CFL number impact the accuracy, stability, and computational efficiency of the simulations.

3.2 Implementing the CFL Number

The study consists of running the same simulation four times with only one parameter changing : The CFL number (by changing the time step Δt)

Table 6: CFL Effect Study Results

Mesh	C_d **(% Change)**	S_{t_L} **(% Change)**	S_{t_D} **(% Change)**	**Comp. Time (core-hours)**
CFL = 1	0.5937 (–)	0.2431 (–)	0.2431 (–)	78.1
CFL = 10	0.6027(1.49%)	0.2390(-1.71%)	0.2390 (-1.72%)	15.4
CFL = 40	0.6131(1.70%)	0.2235(-6.93%)	0.4321 (44.69 %)	6.9
CFL = 100	0.5764(-6.37%)	0.1867(-19.72%)	0.4465 (3.22%)	3.6

Its important to distinguish here the Lift Strouhal Number S_{t_L} from the drag Strouhal Number S_{t_D}. Both represent the normalized characteristic frequency of the flow but respectively, one represents the frequency extracted from the Lift Curve (plotted against

time), and the other from the Drag Curve.
Lets examine the effect of CFL on the different parameters in more detail:

3.2.1 "Drag" Strouhal Number

The effect of CFL on the Drag Strouhal number is undeniably the most interesting and consequential. The inherent relationship between the drag Strouhal number and the behavior of the drag force makes changing the CFL number particularly significant. As discussed previously, when the CFL number exceeds one, the algorithm fails to properly solve the conservation equation in each cell, causing some of the fluid to skip certain cells. This is especially critical in the boundary layer and close to the cylinder wall, which essentially dictates the behavior of the drag force. Therefore, if we cannot accurately model the boundary layer consistently due to a high CFL number, we observe irregular behavior in the drag force, leading to anomalous oscillations and consequently aberrant values for the Strouhal number:

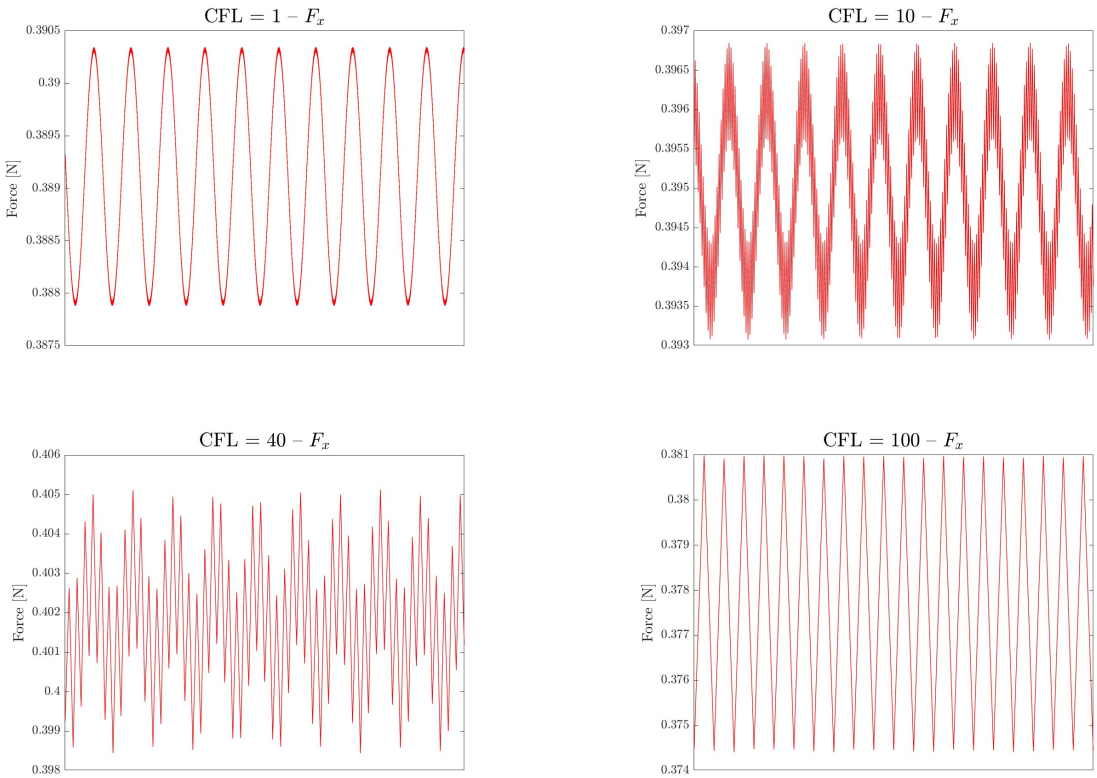

Figure 7: Drag force behavior with different CFL numbers

The above plots depict how drag forces behave with varying CFL numbers. It is evident that higher CFL numbers result in more chaotic, unstable, and irregular outcomes. It appears that as we increase the CFL number, high-frequency oscillations become more pronounced. This trend is illustrated in the following FFT plots:

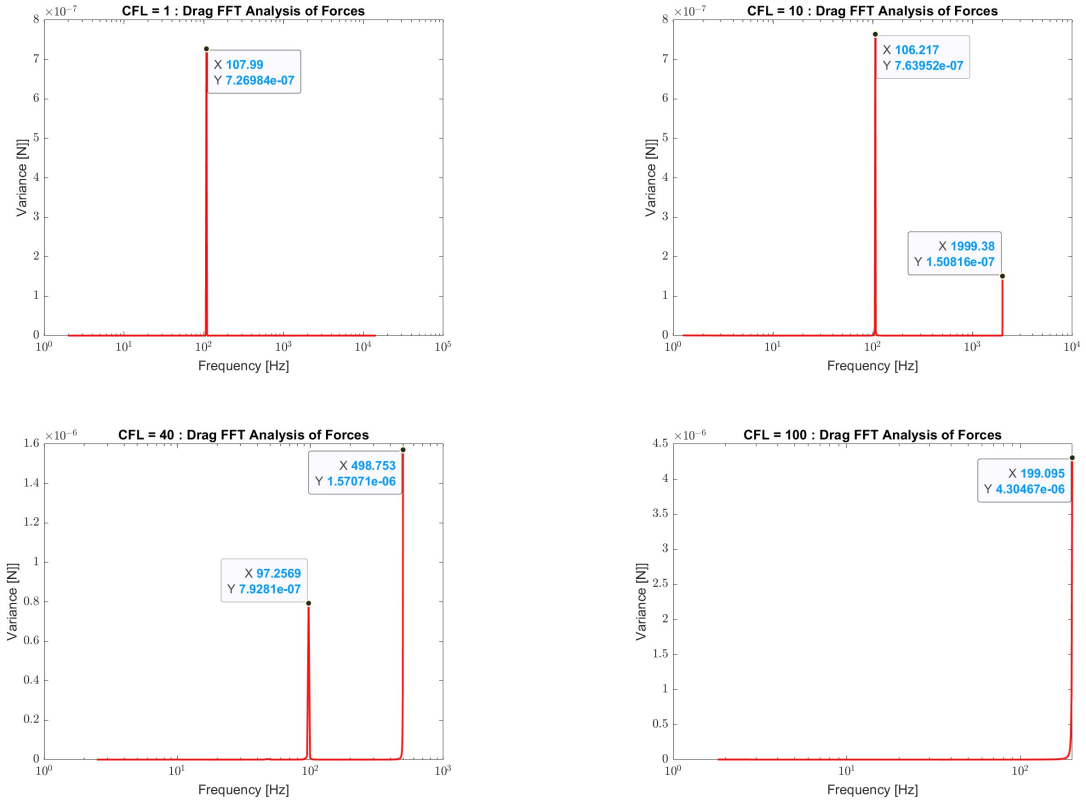

Figure 8: Drag force FFT plots with different CFL numbers

The results demonstrate a clear emergence of a high-frequency term as the CFL number increases. In the case of CFL = 1, only the fundamental low-frequency term is evident. However, as the CFL number rises to 10, a high-frequency term begins to appear, albeit with the low frequency still dominating. By CFL = 40, the high-frequency term becomes dominant, and at CFL = 100, the low-frequency term completely disappears. This phenomenon explains the peculiar spike shape observed in the fourth plot of Figure 7. Furthermore, this observation justifies the significant increase of 45% in the value of S_{t_D} as reported in Table 6. Therefore, there is no doubt that the effect of CFL is to insert these new unstable fast-changing terms in the behaviour of the fluid

3.2.2 Average Drag Coefficient

There isn't anything particularly intriguing in the behavior of the average drag coefficient. Indeed, $\overline{C_d}$ gradually increases with CFL, which could be attributed to the higher frequency terms stimulating the boundary layer more. However, at CFL = 100, we observe a sudden drop. As indicated in the plots, this is likely because the regime or solution that the algorithm converges to is a different nonphysical one, resulting in a different average drag.

3.2.3 "Lift" Strouhal Number

The relationship depicted in this plot is surprisingly linear. Unlike the relationship between S_{t_D} and CFL, which is more complex, the linearity in S_{t_L} versus CFL is likely due to lift being a consequence of a more macro and global phenomenon of vortex shedding. Unlike drag, lift does not heavily rely on the intricacies and details of the boundary layer, which are more local and detailed. This fact becomes evident in this clear relationship. One possible reason for this decreasing relationship is that at high CFL values, the algorithm fails to capture all of the lift detail, skipping some. As a result, overall values become smaller because some of the cells that are supposed to contribute to lift are skipped.

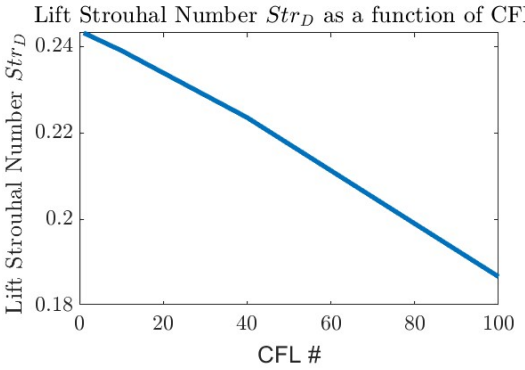

Figure 9: S_{t_L} as a function of CFL number.

3.2.4 Computational Time

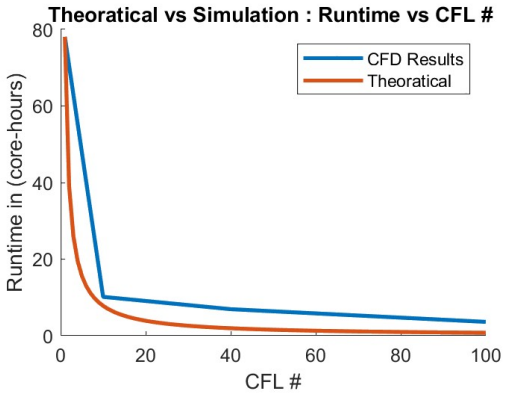

Figure 10: Effect of CFL on runtime

In theory, if we double the CFL number, we expect the simulation to run twice as fast, following a relationship like Runtime $= \frac{\text{const.}}{CFL}$. However, in practice, this ideal relationship doesn't always hold true. Doubling the CFL number doesn't necessarily lead to a simulation that is precisely twice as fast; instead, we often observe a saturation phenomenon. This phenomenon is akin to the difference between parallel and single-core simulations, where increasing computational resources doesn't always linearly improve performance.

4 Effect of Wall Treatment and Turbulence Model Combinations

4.1 Comparison: Spalart-Allmaras vs. k-ω SST Model

The Spalart-Allmaras model and the k-ω SST model are two widely used turbulence models in fluid simulations, each offering unique approaches to capturing turbulent flow phenomena. On one hand the Spalart-Allmaras model solves a single transport equation for turbulent viscosity, ν_t as opposed to the k-ω SST model which combines the k-ω and k-ε turbulence models. Here are some of the key differences:

Key Differences:

- **Equation Complexity:** Spalart-Allmaras model: single transport equation for turbulent viscosity; k-ω SST model: multiple equations for turbulent kinetic energy and specific dissipation rate.
- **Model Applicability:** Spalart-Allmaras: favored for aerodynamics due to efficiency; k-ω SST: offers improved accuracy in complex flows.
- **Treatment of Near-Wall Turbulence:** k-ω SST: resolves near-wall turbulence explicitly; Spalart-Allmaras: models it through a turbulent viscosity transport equation.
- **Computational Cost:** Spalart-Allmaras: lower computational costs compared to k-ω SST.

4.2 Comparison: Wall-Modeled vs. Wall-Resolved

The choice between wall-modeled (WM) and wall-resolved (WR) approaches is crucial in Computational Fluid Dynamics simulations, particularly for flows near solid boundaries (See 2 for more details). Below, we outline the key differences between these approaches:

Wall-Modeled (WM) Approach: In the wall-modeled approach, the near-wall region is not resolved explicitly but instead modeled using turbulence models or wall functions. Turbulence models such as the Spalart-Allmaras model or k-ω SST model are used to capture the turbulence characteristics near the wall. Wall functions provide a computationally efficient way to extrapolate flow variables from the resolved flow domain to the near-wall region, avoiding the need for fine grid resolution near the wall.

Wall-Resolved (WR) Approach: In contrast, the wall-resolved approach resolves the entire boundary layer region with a fine grid, allowing for direct simulation of the flow dynamics near the wall. This approach provides accurate predictions of near-wall turbulence and flow separation but typically requires significantly higher computational resources compared to the wall-modeled approach. Wall-resolved simulations are often preferred for complex flows with intricate boundary layer structures or regions.

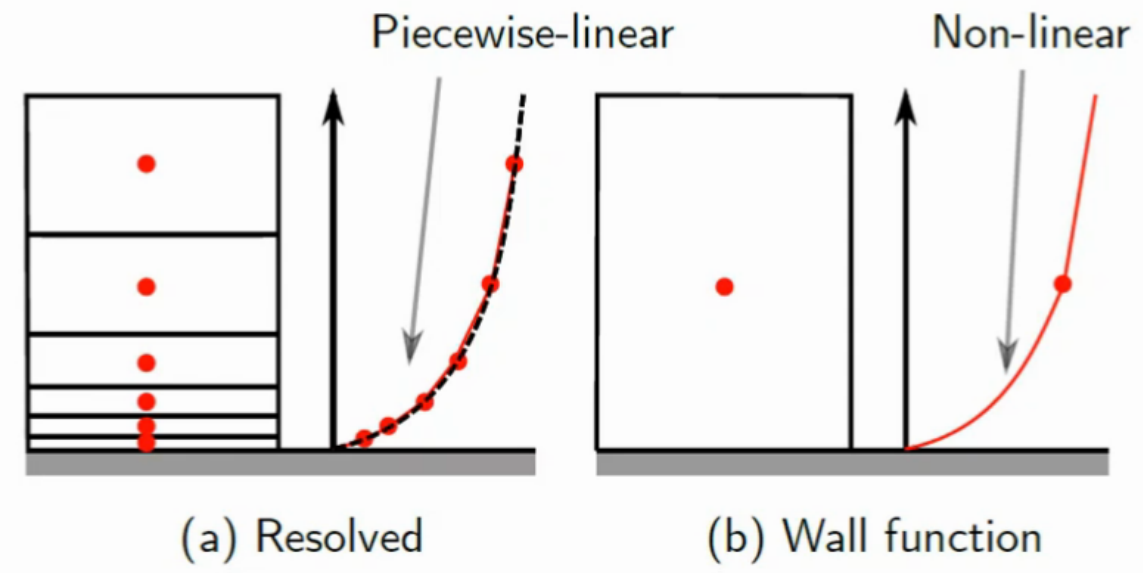

Figure 11: Wall Resolved BL Vs Wall Modeled BL

Key Differences:

- **Computational Cost:** WM is computationally more efficient than WR, making it suitable for large-scale simulations or cases with limited computational resources.
- **Accuracy:** WR offers higher accuracy in capturing near-wall turbulence and flow features compared to WM due to direct resolution of the boundary layer region.
- **Applicability:** WM is commonly used in industrial applications where computational efficiency is paramount, while WR is preferred for research purposes or cases requiring high-fidelity predictions of near-wall flow dynamics.

4.3 Implementation and Evaluation of Various Turbulence Model and Wall Treatment Combinations

With these key concepts in mind, we can now proceed to implement the simulations and analyze their results. To effectively describe and compare the different combinations, we simulated four distinct configurations, each producing unique results:

Table 7: Summary of Simulation Cases

Case	$\overline{C_d}$	S_{t_L}	**Separation Angle**	**Comp. Time (core-hours)**
SA WR	0.5937	0.2431	103.7	78.1
SA WM	1.2836	0.2587	108.1	58.7
SST WR	0.8597	0.2523	112.7	86.0
SST WM	0.8475	0.2854	124.5	74.1

The following table provides the settings used for the models:

Table 8: Turbulence Models Paramters, See 11 & 12 for more details

Turbulence Model	**Wall Setup**
SA	**Wall Resolved**
See 3	
SA	**Wall Modeled**
$\tilde{\nu}$ (Nutilda)	`nutUSpaldingWallFunction`
SST	**Wall Resolved**
Turbulence intensity	0.05
Characteristic length	0.0081
ω (Omega)	`omegaWallFunction`
ν_t (Nut)	`nutLowReWallFunction`
SST	**Wall Modeled**
k	`kqRWallFunction`
ν_t (Nut)	`nutUWallFunction`

A couple of things to point out here:

- **Computational Cost:** For both SA and SST models, the wall-modeled approach is significantly less computationally expensive than the wall-resolved approach. This is expected, as discussed in the previous section, where the wall model bypasses simulating the intricate boundary layer by utilizing empirical results. Additionally, the results show that SST is more computationally demanding than SA.
- **Separation Angle:** The separation angle, for both SA and SST models, is consistently greater for the wall-modeled approach compared to the wall-resolved approach. It appears that the wall function used in wall-modeled simulations overemphasizes viscosity itself, thereby delaying separation. The wall-modeled approach was designed for flow over a flat plate, so its application to a curved surface may not be optimal.

- **Difference in Results:** The difference in results between SA with wall-resolved (WR) versus wall-modeled (WM) approaches is notably large, especially concerning the average drag, which more than nearly doubled. This stark contrast is observed in contrast to the difference between SST with WR and WM approaches, which yields nearly identical drag coefficients.
- **Strouhal Number:** The Strouhal number is generally higher for the SST model compared to the SA model. Additionally, it is almost always significantly higher for a wall-modeled approach compared to a wall-resolved one.

Experimental studies show that the real values of these specific parameters of a an airflow around a cylinder are given by the following [5] [6] [7]:

Case	$\overline{C_d}$	S_{t_L}
EXP	1.0 – 1.2	≈ 0.2

Table 9: Experimental Results

Comparing these results with the test matrix 10, the following can be deduced:

- **Strouhal Number:** All models overshoot the real value by at least 20%. The most inaccurate in terms of Strouhal is the SST Wall Modeled approach with an absolute error of 40%. This inaccuracy is likely attributed to various factors, including insufficient mesh refinement to fully simulate the flow, imperfect turbulence modeling assumptions, or numerical errors and diffusion.
- **Drag**: The results indicate that generally, the SST model is closer to reality. This explains its popularity in both industry and academia, offering a good balance between computational cost and accuracy. Both the WM SST and SST WR perform well in terms of drag, although the SST WM significantly overshoots the Strouhal number.
- **SA Model:** The SA WM approach slightly overpredicts the drag, with a value around 1.3. Overall, it seems to be an acceptable approach based on these results, as both the drag and Strouhal numbers exhibit acceptable absolute errors relative to the experiments. On the other hand, the SA WR surprisingly performs worse than the SA WM, with a significant undershoot of the drag coefficient at around 0.6 (nearly a 50% error). Therefore, under these conditions, it's not a very accurate model.

To further deepen the understanding, knowledge, and interpretation of these numbers, an analysis of the pressure coefficient distribution $C_{p_{avg}}$ and y_+ distribution on the cylinder wall surface is provided, coupled with an analysis of the wake of the cylinder at a distance of 0.02 from the center of the cylinder (Turbulence Intensity and average speed):

4.3.1 Cylinder Wall Surface Analysis

The 2 following provide more insight into the way pressure is distributed and the y_+ (for the wall modeled simulations) values of the cylinder wall surface:

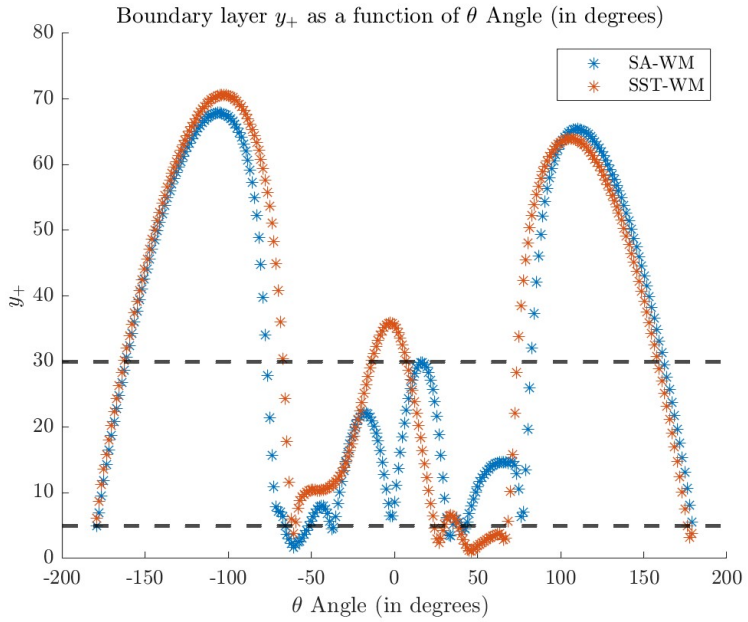

Figure 12: y_+ Distribution around Cylinder Wall

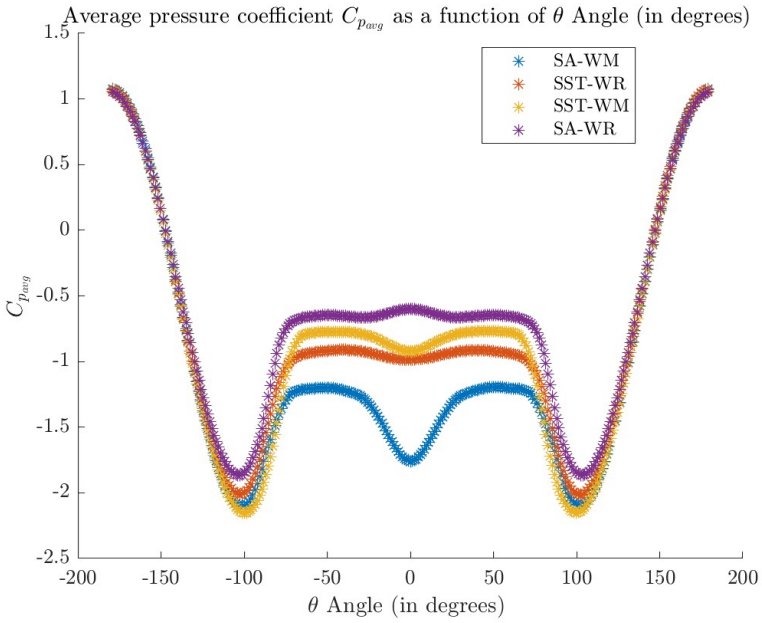

Figure 13: C_p Distribution around Cylinder Wall

The following can be said :

- As depicted in the y_+ plot, a significant portion of the boundary layer ($\theta = [-50°; 50°]$) falls within the troublesome y_+ range of $[5; 30]$, which is unpredictable and challenging to model. This observation is crucial to consider and may help explain discrepancies in some of the results.

- Examining the C_p plot, we observe overall similarity in the solutions, except within the interval $[-100°; 100°]$, where separation occurs. Within this interval, a correlation between the average drag coefficient $\overline{C_d}$ and the pressure coefficient is evident (notably with SA WR exhibiting the top curve (purple) and SA WM the blue curve). The drag force is influenced by pressure differences, where a lower curve (blue) indicates a higher pressure difference and more suction behind the cylinder, resulting in a higher drag coefficient.

- Finally, analyzing the pressure plot, we notice an anomalous behavior in the SA-WR model, where there is a spike at $0°$(in contrast to a dip observed in the other models). This behavior is nonphysical, as $\theta = 0$ represents the back of the cylinder where pressure is not expected to increase as seen in this spike. This anomaly might elucidate why the drag of the SA WR model is notably low.

4.3.2 Analysis of Cylinder Wake Properties

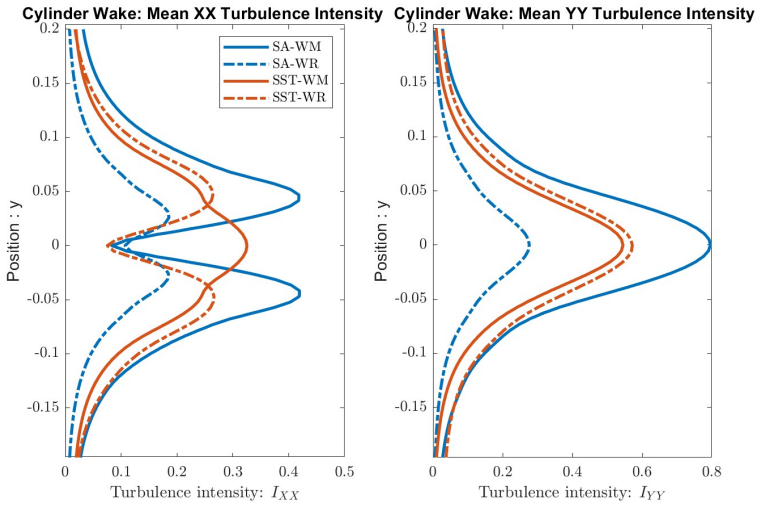

Figure 14: Wake Profile : U_{xx} and U_{yy}

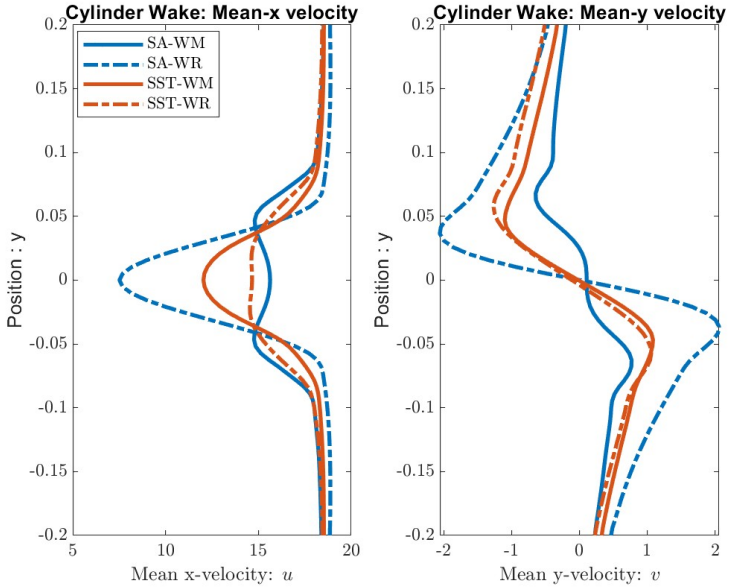

Figure 15: Wake Profile: Average Velocity

- Analyzing the plots for turbulence intensity, there is a clear correlation between turbulence intensity and $\overline{C_d}$. The higher the intensity (for a respective model), the higher the drag coefficient.
- Regarding the yy component of turbulence intensity, all the models exhibit similar trends, albeit with variations in scale. However, for the xx component of turbulence intensity, the SST-WM approach stands out with a distinct shape. This discrepancy is likely attributed to the assumptions of the Wall function. It's noteworthy that this model coincides with the highest separation angle, indicating potential anomalies in the boundary layer and its underlying assumptions.
- When examining the mean values of speed, no significant trend or correlation is immediately evident. However, it's notable how the SA WR differs from SA WM in the plots. Additionally, there's asymmetry in the mean y plot, likely stemming from the chosen position for wake analysis (0.02m behind the cylinder). At this specific point, the average vortex shape predominantly exhibits clockwise rotation.

5 Conclusions and Final Verdict

In conclusion, when conducting an unsteady CFD simulation, it's crucial to monitor a plethora of parameters and assumptions while keeping in mind the end goal of the application or simulation.

One key takeaway from this study is that for unsteady CFD simulations, the CFL number should always be kept under 1 to avoid numerical instability and the appearance of high-frequency terms in the solutions.

Another critical consideration is the choice of turbulence model. Some models are more finely tuned for specific cases compared to others. It's important to examine similar simulation setups and understand the reasoning behind the selection of turbulence models. Certain models may be better adapted for the particular landscape of the simulations.

Furthermore, it's essential to approach Wall-Modeled (WM) approaches with caution. While they offer computational time savings, there is often a trade-off in solution accuracy. Prioritizing whether runtime or accuracy is more important in the specific simulation case is crucial.

Finally, it's important to be careful and to note that CFD simulations are highly complex, with dozens of variables to fine-tune and adjust in order to obtain accurate results. Verifying the solutions is crucial to ensure correctness. CFD should be assumed guilty before being innocent, and not the other way around.

6 Appendix

Case	**Residual Values**				**T.Step (s)**	**Runtime (in C-h)**	$y_{+_{max}}$	$\bar{y}_+$	$\overline{CFL}$	$CFL_{\max}$
	Pressure p	x **velocity** u	y **velocity** v	**Turb Viscosity** $\tilde{\nu}$						
Grid Convergence Test										
Coarse	9.77544e-07	1.1791e-10	5.6026e-10	3.89043e-09	5e-5	24.7	2.2	1.15	0.07	0.99
Medium	9.2556e-07	1.43284e-10	5.29731e-10	5.2547e-09	5e-5	34.0	1.94	1.02	0.094	1.52
Medium-2	**9.93323e-07**	**1.80424e-10**	**7.41036e-10**	**6.13915e-09**	**3.5e-5**	**78.1**	**1.86**	**0.96**	**0.095**	**1.43**
Fine	8.38215e-07	2.04121e-10	6.67312e-10	8.99063e-09	1e-5	190.6	1.81	0.90	0.071	1.12
Effect of CFL #										
CFL = 1	9.93323e-07	1.80424e-10	7.41036e-10	6.13915e-09	3.5e-5	78.1	1.86	0.96	0.095	1.43
CFL = 10	1.6093e-06	1.1660e-06	2.0003e-06	3.1777e-05	3.5e-5	10.1	1.93	0.94	0.68	10.28
CFL=40	6.6605e-07	2.1527e-07	2.4346e-07	5.7221e-06	3.5e-5	6.9	1.84	0.95	2.71	40.73
CFL=100	1.6316e-07	1.5282e-07	1.5393e-07	3.5209e-06	3.5e-5	3.6	1.96	0.89	6.68	98.98
Turbulence And Wall Treatment Effects										
WR SA	9.93323e-07	1.80424e-10	7.41036e-10	6.13915e-09	3.5e-5	78.1	1.86	0.96	0.095	1.43
WM SA	5.91912e-07	1.23074e-09	1.00063e-09	2.36742e-09	3.5e-5	58.7	67.9	32.5	0.098	1.19
WR SST	9.18727e-07	1.32999e-09	1.44487e-09	k=4.20619e-09 ω=2.63452e-09	2e-5	86.0	2.00	1.08	0.055	0.87
WM SST	7.45294e-07	2.15456e-09	1.04487e-09	k=9.30589e-09 ω=3.23508e-09	2e-5	74.1	70.6	35.2	0.055	0.70

Table 10: Summary of Residuals, Convergence, y^+, and CFL

6.1 Spalart-Allmaras Model

The Spalart-Allmaras model, and is given by:

$$\frac{\partial(\rho\tilde{\nu})}{\partial t} + \nabla \cdot (\rho\tilde{\nu}\mathbf{u}) = \nabla \cdot \left[\left(\frac{\nu}{\sigma_\nu} + \frac{\nu_t}{\sigma_{\nu_t}} \right) \nabla\tilde{\nu} \right] + S_\nu + S_{\nu_t} \tag{2}$$

where $\tilde{\nu}$ represents the turbulent viscosity, $\mathbf{u}$ is the velocity vector, ν is the kinematic viscosity, ρ is the density, and σ_ν and σ_{ν_t} are model constants.

6.2 k-ω SST Model

The k-ω SST model combines the k-ω and k-ε turbulence models and is expressed as:

$$\frac{\partial k}{\partial t} + \mathbf{u} \cdot \nabla k = P - \beta^* \rho k\omega + \nabla \cdot [(\nu + \sigma_k\tilde{\nu})\nabla k]$$

$$\frac{\partial \omega}{\partial t} + \mathbf{u} \cdot \nabla \omega = \frac{\gamma}{\nu} P - \beta\rho\omega^2 + \frac{1}{\sigma_\omega} \nabla \cdot [(\nu + \sigma_\omega\tilde{\nu})\nabla\omega] + 2(1 - F_1)\frac{\omega}{k}\frac{\partial k}{\partial x}$$

where k is the turbulent kinetic energy, ω is the specific dissipation rate, ν is the kinematic viscosity, ρ is the density, P represents the production term, and σ_k, σ_ω, β, β^*, γ, F_1 are model constants.

Table 11: Initial and Boundary Conditions for SA Turbulence models

Parameter	**Value**
Initial Conditions	
internalField	
ν_t	Uniform : $1.4 \times 10^{-5}\,\mathrm{m}^2/\mathrm{s}$
$\tilde{\nu}$	Uniform : $5.5 \times 10^{-5}\,\mathrm{m}^2/\mathrm{s}$
Boundary Conditions	
Inlet	
Boundary Type	Patch
ν_t BC	Calculated
$\tilde{\nu}$ BC	FixedValue: $5.5 \times 10^{-5}\,\mathrm{m}^2/\mathrm{s}$
Outlet	
Boundary Type	Patch
ν_t BC	Calculated
$\tilde{\nu}$ BC	ZeroGradient
Wall	
Boundary Type	Wall
$\tilde{\nu}$ BC	FixedValue: 0
For WM: $\tilde{\nu}$ BC	nutUSpaldingWallFunction
ν_t BC	FixedValue: 0
For WM: ν_t BC	nutUSpaldingWallFunction
Top and Bottom	
Boundary Type	Patch
$\tilde{\nu}$ BC	ZeroGradient
ν_t BC	Calculated,
Sides	
Boundary Type	Empty
$\tilde{\nu}$ BC	Empty
ν_t BC	Empty

Table 12: Initial and Boundary Conditions for KW SST Model

Parameter	**Value**
Initial Conditions	
internalField	
ν_t	Uniform: $1.4 \times 10^{-5}\,\mathrm{m}^2/\mathrm{s}$
k	Uniform: $1.2231135\,\mathrm{m}^2/\mathrm{s}$
ω	Uniform: $15.02995326\,\mathrm{s}^{-1}$
Boundary Conditions	
Inlet	
Boundary Type	Patch
ν_t BC	Calculated
k BC	FixedValue: $1.2231135\,\mathrm{m}^2/\mathrm{s}$
ω BC	FixedValue: $15.02995326\,\mathrm{s}^{-1}$
Outlet	
Boundary Type	Patch
ν_t BC	Calculated
k BC	zeroGradient
ω BC	ZeroGradient
Wall	
Boundary Type	Wall
ν_t BC	nutLowReWallFunction
k BC	FixedValue: $0\,\mathrm{m}^2/\mathrm{s}$
ω BC	omegaWallFunction
For WM: ν_t BC	nutUWallFunction
For WM: k BC	kqRWallFunction
For WM: ω BC	omegaWallFunction
Top and Bottom	
Boundary Type	Patch
ν_t BC	Calculated
k BC	ZeroGradient
ω BC	ZeroGradient
Sides	
Boundary Type	Empty
ν_t BC	Empty
k BC	Empty
ω BC	Empty

References

[1] NASA. (2014) Flow past a cylinder. NASA. [Online]. Available: https://www.grc.nasa.gov/WWW/k-12/airplane/Images/flowcyl.jpg

[2] OpenFOAM. (2018) Openfoam: User guide v2112. OpenCFD Ltd. [Online]. Available: https://www.openfoam.com/documentation/guides/latest/doc/guide-applications-solvers-incompressible-simpleFoam.html

[3] ——. (2018) Openfoam: User guide v2112. OpenCFD Ltd. [Online]. Available: https://www.openfoam.com/documentation/guides/latest/doc/guide-applications-solvers-incompressible-pimpleFoam.html

[4] ——. (2024) A.1 standard solvers. OpenCFD Ltd. [Online]. Available: https://www.openfoam.com/documentation/user-guide/a-reference/a.1-standard-solvers

[5] W. D. Aurelien Borgoltz and N. Intaratep. (2021) Experiment 3 - flow past a circular cylinderr. Virgina Tech AOE 3054. [Online]. Available: https://borgoltz.aoe.vt.edu/aoe3054/manual/expt3/index.html

[6] OrcaFlex. Line types: Drag and lift data. OrcaFlex. [Online]. Available: https://www.orcina.com/webhelp/OrcaFlex/Content/html/Linetypes,Dragliftdata.htm

[7] B. K. S. R. C. L. Y. B. A. Cox, Jared S. (1997) Computation of vortex shedding and radiated sound for a circular cylinder. NASA. [Online]. Available: https://ntrs.nasa.gov/api/citations/20040110243/downloads/20040110243.pdf